Jules Malavieille L3 SVT Mer

Regime shift : dynamic and prevision by a stochastical model

Internship with Jean-Christophe Poggiale summer 2024

Table des matières

1 Abstract

During this internship, we used a continuous-time stochastic model to study tipping points in ecosystems. Through the analysis of this model, we highlighted that stochastic systems—being closer to real-world dynamics—tend to shift earlier than predicted by their deterministic counterparts. We also observed a rise in variance and autocorrelation prior to the transition. However, these early warning methods are often unusable in practice due to their reliance on "future" data, which limits their ability to anticipate regime shifts in real ecosystems.

2 Introduction

A tipping point refers to the moment when an ecosystem abruptly shifts from state A to state B in response to the slow and continuous variation of a system parameter. Typically, state A is characterized by high biomass (a high-density state), while state B corresponds to a lower biomass (a low-density state). These transitions often reduce the productivity of ecosystems and raise critical issues in terms of conservation, with social, economic, or even political implications. Anticipating such shifts is therefore a key aspect of managing and protecting ecosystems prone to these transitions.

Our case study focuses on the spruce budworm model, a parasite that can kill large numbers of trees and cause a spruce forest (the high-density state) to collapse into a grassland (the low-density state). The dynamics are described by a continuous-time stochastic model, which cannot be solved analytically but can be approximated numerically. While analytically intractable, this stochastic formulation better reflects the inherent randomness of ecological systems compared to deterministic models.

The objective of this internship was to explore numerical approximation methods for stochastic differential equations (SDEs) applied to population dynamics, to compare them with deterministic models, and to evaluate the performance of early warning signals (EWS) on these stochastic systems. In short, we asked : are stochastic models consistent with their deterministic counterparts, and can they be used to anticipate tipping points in ecosystems ?

3 Materials and Methods

3.1 Principles of Tipping Points in Ecosystems

The concept of tipping points in ecosystems can be summarized by Figure 1 :

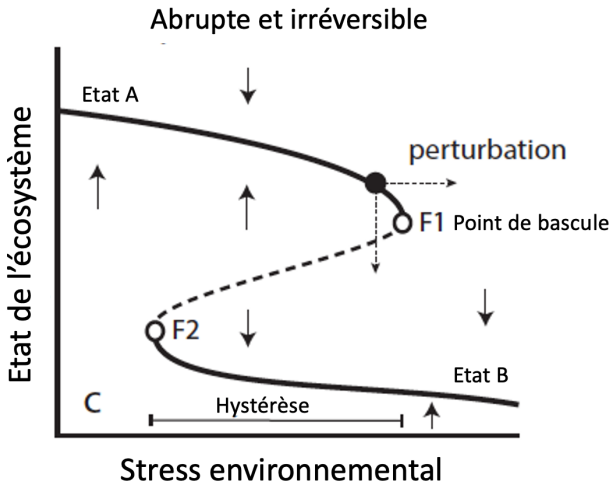

FIGURE 1 – Scheme of a tipping point. Modified from (V. Dakos, 2022)

Figure 1 shows that the system is composed of two stable equilibria : A, a high-density state, and B, a low-density state. If environmental stress increases, the system shifts from state A to B—this is referred to as a tipping point. F_1 represents the theoretical tipping point from A to B, and F_2 the tipping point from B to A. This reversible shift between two states is called hysteresis.

When referring to environmental stress, we are more precisely describing the variation of one of the system's parameters that, once a threshold is crossed, triggers a disturbance pushing the system toward the low-density state. This is known as a driver parameter (V. Dakos, 2022).

These shifts are characterized by abrupt dynamics and occur very rapidly once the driver's threshold value is exceeded. Moreover, they are often irreversible. It is therefore critical to be able to anticipate their occurrence in order to prevent transitions to states that are less favorable for human interests.

For instance, in the Mediterranean Sea, forests of *Cystoseira sp.*—which play an important role in trophic networks and serve as nursery habitats for many species (Steneck et al., 2002)—can become barren ground within a few years if predation by *Paracentrotus lividus* becomes too intense. This leads to a far less productive and diverse ecosystem (Thibaut et al., 2005, 2015).

3.2 Spruce Worm Model

$$\frac{dN}{dT} = RN(1 - \frac{N}{K}) - \frac{AN^2}{B^2 + N^2}P + bW \tag{1}$$

Symbol	Parameters	Units
N	Number of spruce worms	individuals
R	Growth rate of the worm	j^{-1}
K	Carrying capacity of the environment	individuals
A	Predation rate on the worm	j^{-1}
B	Half-saturation coefficient	individuals
P	Quantity of predators	individuals
b	Noise regulation coefficient	unitless
W	White noise	$ind \cdot j^{-1}$

TABLE 1 – Parameters and units of the spruce worm model

This model is a continuous-time model. It contains a deterministic part : $RN\left(1 - \frac{N}{K}\right) - \frac{AN^2}{B^2+N^2}P$. The worm population grows according to $RN\left(1 - \frac{N}{K}\right)$ (logistic growth) and is reduced by predation through $\frac{AN^2}{B^2+N^2}P$.
The model also includes a stochastic component bW, which simulates the natural environment more realistically. Here, W is a white noise term (standard normal distribution), and b is a coefficient that scales the effect of the noise.
In order to simplify this model, we perform a nondimensionalization using $x = \frac{N}{B}$ and a time change $T = \frac{AP}{B}t$ (see Appendix 1). This leads to the following dimensionless model :

$$\frac{dx}{dt} = rx(1 - \frac{x}{K}) - \frac{x^2}{1 + x^2} + bW \tag{2}$$

The model now depends only on two parameters : r, the growth rate of the spruce worm, and K, the carrying capacity of the environment. This simplification eases the following steps, particularly the calculation of equilibria.
To proceed, we solve the deterministic part of the system :

$$\frac{dx}{dt} = 0$$

$$rx(1 - \frac{x}{K}) - \frac{x^2}{1+x^2} = 0$$

$$\text{So } x = 0 \text{ ou } r(1 - \frac{x}{K}) - \frac{x}{1+x^2} = 0$$

We now define the functions $f(x) = r\left(1 - \frac{x}{K}\right)$ and $g(x) = \frac{x}{1+x^2}$. By plotting these two functions with respect to x, we can identify the equilibria and their stability graphically. Stability is determined by the condition that the slope at the equilibrium point X is negative, i.e., $X < 0$. We distinguish three possible cases in our model :

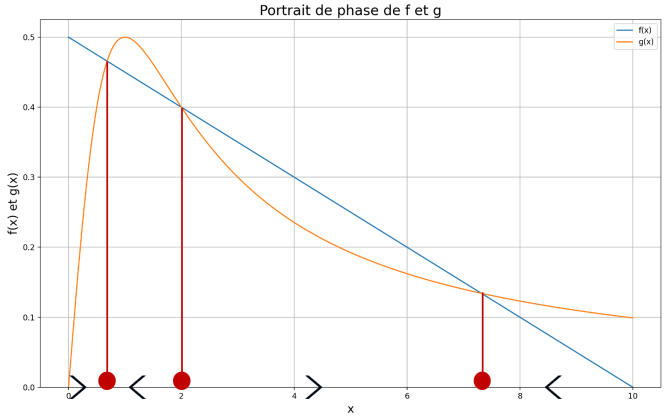

FIGURE 2 – Phase portrait with three equilibria. Red dots indicate the equilibria, black chevrons indicate their stability. The orange curve is $g(x)$ and the blue curve is $f(x)$.

In Figure 2, we observe that the intercept of $f(x)$ at the origin controls the existence of equilibria. This intercept corresponds to the parameter r, which thus drives the state of the system ; it is the driver parameter. For the value of r shown, we observe three equilibria : a low-density and a high-density stable equilibrium, separated by an intermediate unstable equilibrium. In this case, if the value of x is greater than the intermediate equilibrium, the system evolves toward the high-density state, and if it is lower, toward the low-density state.

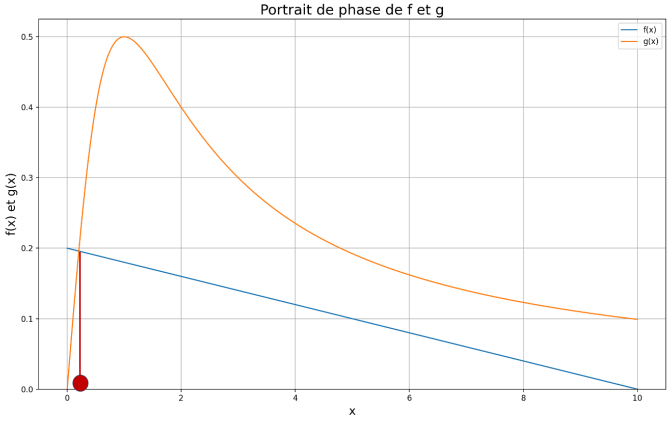

FIGURE 3 – Phase portrait showing only the low-density equilibrium. The red dot is the stable equilibrium. The orange curve is $g(x)$ and the blue curve is $f(x)$.

In Figure 3, the value of r is lower than in the previous case. The system then has only one equilibrium point, which is the stable low-density equilibrium.
In Figure 4, the value of r is higher than in the first case. The system then has only one equilibrium

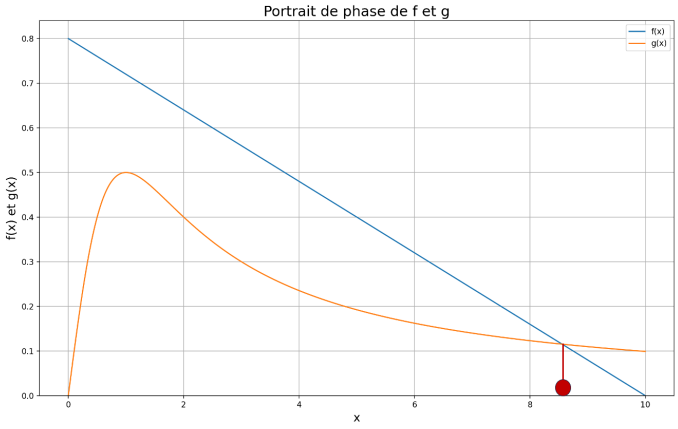

FIGURE 4 – Phase portrait showing only the high-density equilibrium. The red dot is the stable equilibrium. The orange curve is $g(x)$ and the blue curve is $f(x)$.

point : the stable high-density equilibrium.

To study the dynamics of this system, it is necessary to solve it. Since we are dealing with a differential equation, we need to compute its derivative. However, because the model is stochastic, it has no true tangent at any point and is therefore not differentiable in the classical sense. As a result, we must approximate the model using numerical schemes to get closer to a solution.

3.3 Model resolution using the Euler–Maruyama scheme

The first scheme we will test is the Euler–Maruyama scheme. The idea is to separate the equation into two parts : a deterministic part denoted $f(x)$ and a stochastic part denoted $g(x)$. The scheme is then applied according to (J. Higham, 2001) :

$$X_j = X_{j-1} + f(X_{j-1})\Delta t + g(X_{j-1})(W(t_j) - W(t_{j-1})) \tag{3}$$

with

$$W(tj+1) - W(tj) = \sum_{k=jR-R+1}^{jR} W_k \tag{4}$$

To test this scheme, we use a stochastic differential equation that admits an analytical solution :

$$dX = aXdt + bXdW \tag{5}$$

solved by

$$X(t) = X_0 e^{at - \frac{b^2}{2}t} + bW(t) \tag{6}$$

When plotting the solution of this equation, we obviously obtain different curves each time due to the stochastic component. Here is an example of a possible outcome (Figure 5) :

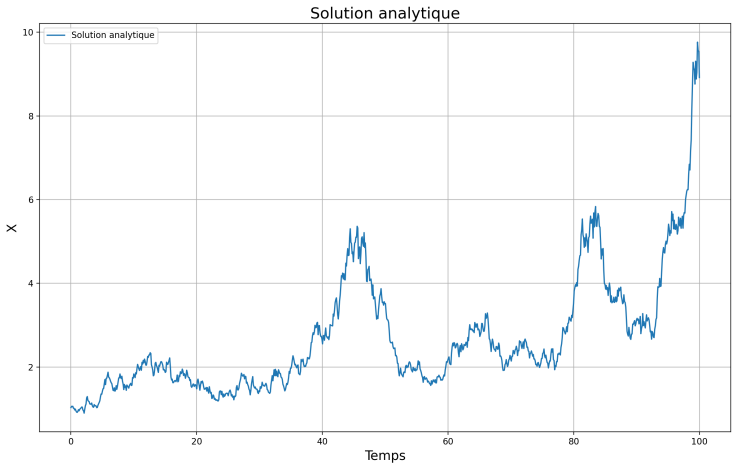

FIGURE 5 – Analytical solution of $dX = aXdt + bXdW$ with W as white noise, and a, b model parameters

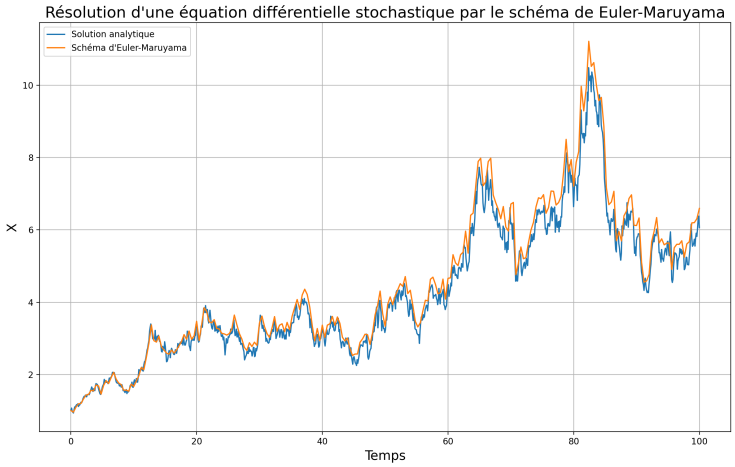

FIGURE 6 – Approximation of the analytical solution (blue) using the Euler-Maruyama scheme (orange) for the model presented in Equation 5

In Figure 6, we use the Euler-Maruyama scheme to approximate this analytical solution. The scheme provides a reasonably good approximation of Equation 5. However, over the entire trajectory, the error remains significant enough to introduce considerable bias. Therefore, it is worth

testing a more accurate scheme that reduces this error. We will now try the Milstein scheme.

3.4 Solving the model using the Milstein scheme

Unlike the previous one, the Milstein scheme is based on a higher-order Taylor expansion, which reduces the error introduced by the first scheme. The Milstein scheme is given by (J. Higham, 2001) :

$$X_j = X_{j-1} + \Delta t f(X_{j-1}) + g(X_{j-1})(W(t_j) - W(t_{j-1})) + \frac{1}{2} g(X_{j-1}) g'(X_{j-1})((W(t_j) - W(t_{j-1}))^2 - \Delta t) \tag{7}$$

Note that the term $W(t_j) - W(t_{j-1})$ is the same as before. We then compare this approximation with both the analytical solution and the Euler-Maruyama scheme.

Figure 7 shows that the Milstein scheme is nearly superimposed on the analytical solution, with a zoom provided for better comparison. The reduced error allows for a much more accurate approximation than the Euler-Maruyama scheme. Therefore, we will retain the Milstein scheme to approximate the spruce budworm model.

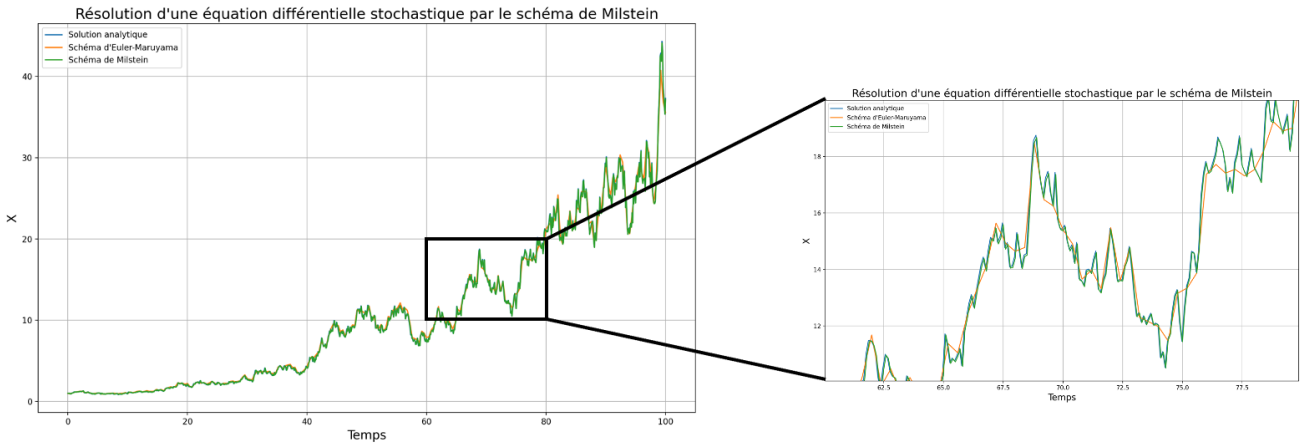

FIGURE 7 – Approximation of the analytical solution (blue) using the Milstein scheme (green), compared with the Euler-Maruyama scheme (orange). The right-hand panel is a zoom of the left-hand panel to better visualize the difference between the analytical solution and the Milstein scheme.

We now apply the Milstein scheme to the spruce budworm model. We define $f(x)$, the deterministic part of the model, as $rx(1 - \frac{x}{K}) - \frac{x^2}{1+x^2}$, and $g(x)$, the stochastic part, as bW. An approximation of the model using the Milstein scheme is shown in Figure 8 for the parameter values $r = 1$ and $K = 10$. Since the model is stochastic, its output varies between simulations.

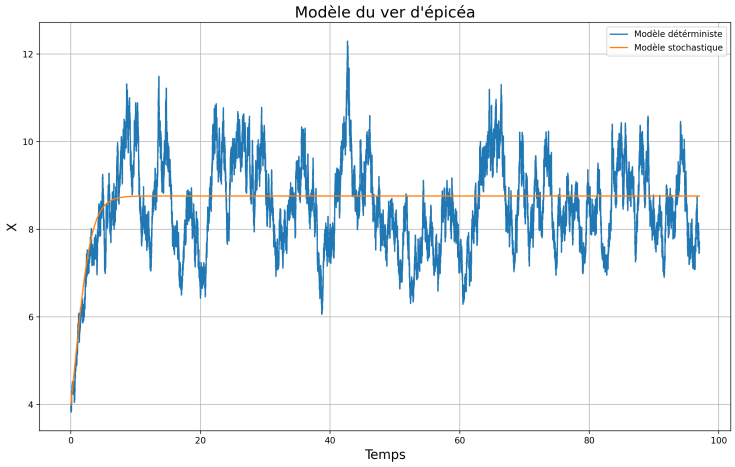

FIGURE 8 – Approximation of the spruce budworm model using the Milstein scheme (blue), compared to the deterministic solution of the model (orange), for $r = 1$, $K = 10$, and W as white noise.

As a final verification of the validity of the Milstein scheme, we compare the stochastic model approximation with its deterministic solution (see Figure 8). We observe that the dynamics of the stochastic model follow the deterministic model's trend, aside from stochastic fluctuations. We will therefore use the Milstein scheme to approximate the spruce budworm stochastic model.

3.5 Tipping point parameters of the model

To determine the conditions under which the spruce budworm model transitions to one equilibrium or another, we must compute its tipping point parameters. A graphical method is available which consists of plotting $r(K)$. To do this, we define x^* as the value of x for which the condition $r(1-\frac{x^*}{K}) = \frac{x^*}{1+x^{*2}}$ is satisfied. This corresponds to the point at which $f(x^*)$ and $g(x^*)$ have no more differential dynamics with respect to each other, meaning that $\frac{d(r(1-\frac{x^*}{K}))}{dx^*} = \frac{d(\frac{x^*}{1+x^{*2}})}{dx^*}$. We can then define the system :

$$\begin{cases} r(1-\frac{x^*}{K}) = \frac{x^*}{1+x^{*2}} \\ \\ \frac{d(r(1-\frac{x^*}{K}))}{dx^*} = \frac{d(\frac{x^*}{1+x^{*2}})}{dx^*} \end{cases} \tag{8}$$

We then obtain (see Appendix 2) :

$$\begin{cases} K &= \frac{2x^{*3}}{x^{*2}-1} \\ \\ r &= \frac{-2x^{*3}(-1+x^{*2})}{(1-x^{*2})(1+x^{*2})^2} \end{cases} \tag{9}$$

We now know the values of r and K, which we can plot for all values of x. This yields Figure 9.

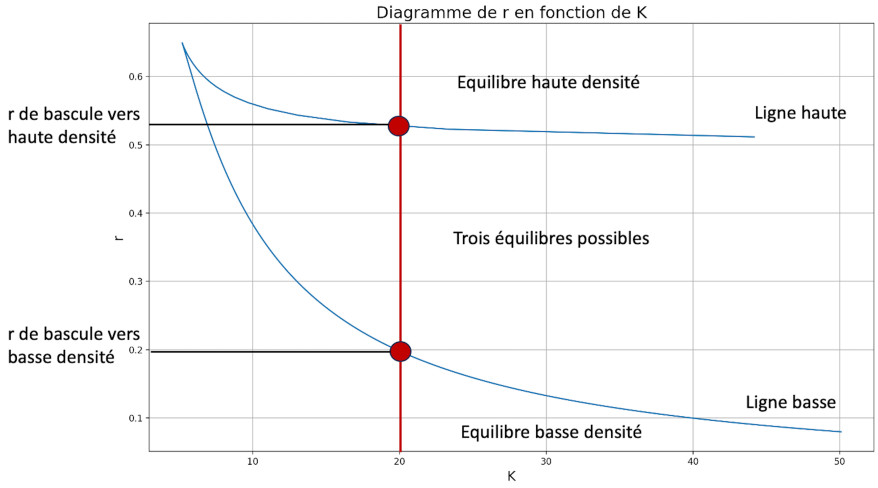

FIGURE 9 – Diagram of r as a function of K (blue) with $x = K$ (red), used to determine the tipping points for the case where $x = K$.

The $r(K)$ curve (see Figure 9) represents the theoretical tipping points for a given K. If r is above the upper curve for a given K, then only the high-density equilibrium exists. If r is below the lower curve for that K, only the low-density equilibrium exists. Finally, if r lies between the upper and lower curves, all three equilibria coexist. The intersection points between the line $x = K$ and the graph represent the tipping points toward high-density equilibrium (upper curve) and low-density

equilibrium (lower curve) for the K corresponding to $x = K$.

We can then visualize this tipping behavior by slightly varying r during a simulation and observing at which value of r the system transitions between equilibria. This can be done with both the stochastic and deterministic models in order to compare their dynamics.

3.6 Tipping point anticipation methods

The ultimate goal of studying tipping points is to be able to anticipate them before an ecosystem transitions to a state that is not favorable for humans. To achieve this, we apply different early warning techniques to our stochastic model and evaluate their performance in a setting close to real data.

3.6.1 Increasing variance

The first strategy is to observe how the system's variance behaves as it approaches a tipping point. As the system nears this point, its resilience decreases (V. Dakos, 2022), meaning it attracts trajectories less strongly to the deterministic path, leading to an increase in variance. Indeed, if we consider $X_{t+1} = aX_t + \sigma\epsilon_t$, the variance reaches its maximum when $a = 1$, which corresponds to the model's critical tipping condition (see Appendix 3). Only, the main issue when working with real-world ecological time series is that we typically have access to only one realization. Therefore, it is not possible to compute variance across many trajectories for each time step. To address this, we compute a rolling (moving) variance. However, if the time series has a trend (increasing or decreasing), it can bias the variance computation. To solve this, we subtract the moving average (computed with a symmetric window) from the series to obtain its residuals. Then we compute the rolling variance of the residuals with a symmetric window as well. If this moving variance increases, it may indicate an approaching tipping point.

3.6.2 Increasing autocorrelation

As mentioned earlier, when the system approaches a tipping point, its resilience decreases. This causes the trajectories to deviate further from the deterministic path, meaning the noise becomes more influential and more autocorrelated. Therefore, the autocorrelation of the residuals increases as the system nears the tipping point. To observe this, we can visualize a lag plot of the time series, plotting X_t against X_{t-1}. As the system nears the tipping point, the points align more closely along the $y = x$ line. The more clustered and aligned the points are, the closer the system is to a bifurcation. This method is particularly useful for real-world data, where only a single time series is available.

4 Results and Discussion

4.1 Comparison between stochastic and deterministic dynamics

Using the method described in Section 3.5 (see Figure 9), we found by visual inspection that for $K = 10$ (used for all subsequent simulations), the theoretical tipping point toward the low-density equilibrium occurs at $r = 0.3840$. Similarly, the tipping point toward the high-density equilibrium occurs at $r = 0.5598$. These values correspond to the bifurcation thresholds predicted by the deterministic model.

We now aim to compare these deterministic tipping values with the ones obtained from the stochastic model. To do this, we simulate both the stochastic and deterministic models, gradually increasing the driver parameter r over time. However, due to random fluctuations in the stochastic model, the tipping values will vary between simulations. Therefore, we run 1000 simulations of the stochastic model to estimate the average tipping point (see Figure 10).

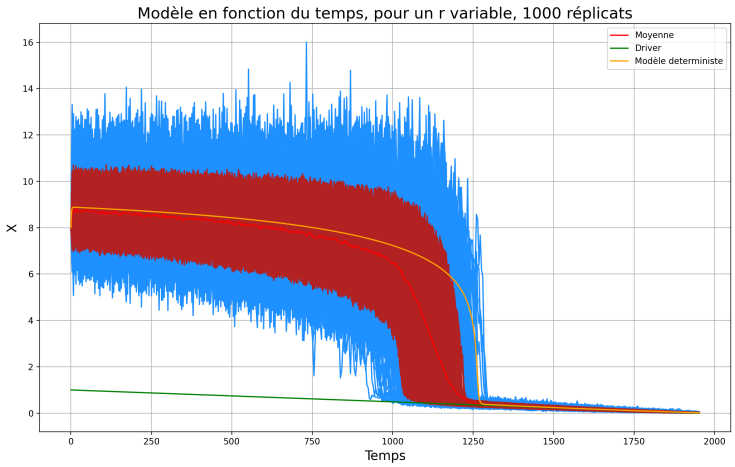

FIGURE 10 – Plot of 1000 simulated trajectories of the stochastic model (blue), with 5%-95% quantiles (dark red), the average of the 1000 series (light red), the driver parameter r (green), and the deterministic model (orange).

In Figure 10, we observe that across 1000 replicates, the average tipping point of the stochastic model toward the low-density equilibrium occurs at $r \approx 0.45$. This is about 0.07 higher than the deterministic tipping point. This difference arises because, as the system approaches the bifurcation point, its resilience weakens, making the trajectories more susceptible to noise. Consequently, the system may switch to the low-density state earlier than predicted by the deterministic model. This result shows that the stochastic model, which is more realistic, tips earlier than the theoretical deterministic threshold. It would be interesting to investigate whether this phenomenon holds true in real-world ecological systems.

4.2 Testing early warning indicators

4.2.1 Rising moving variance of residuals

To better replicate real-world data conditions, we compute variance based on a single time series—just as one would do with actual ecological data. We calculate the moving variance using a symmetric window around each value.

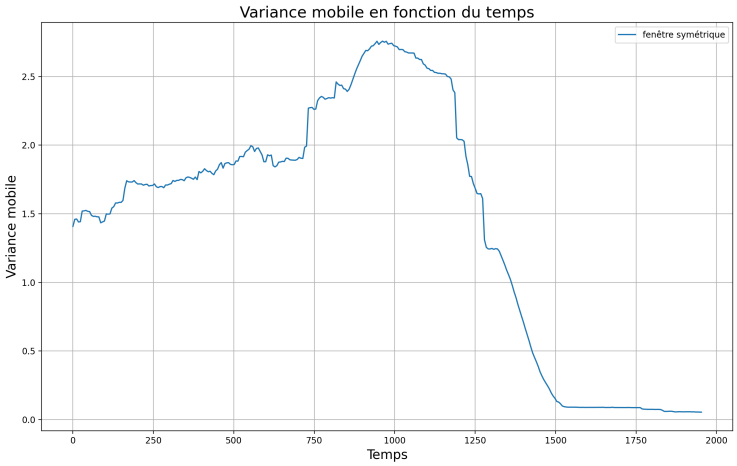

FIGURE 11 – Moving variance computed over one of the 1000 simulated stochastic series.

In Figure 11, we observe the moving variance over an example trajectory. The variance increases until it reaches a plateau, which corresponds to the tipping point. Then, it decreases sharply, nearing zero after the transition. This confirms that the variance increases as the system approaches the tipping point. However, to realistically assess the utility of this method, we must repeat the analysis on a time series where the tipping point has not yet occurred.

Figure 12 presents such a case : the tipping point has not yet occurred. We observe that the variance increases as the system approaches the bifurcation point, even though the shift has not yet happened. However, several limitations arise. The moving window used to compute the variance is symmetric, meaning that it requires "future" data points to compute each centered variance value. This causes a lag between the variance estimated from the time series and the "actual" variance of the ecosystem. The last known variance value will correspond to the last point where the symmetric window fits entirely within the data. One possible solution is to replace the symmetric window with an asymmetric one that looks only into the past.

In Figure 13, we observe that the variance computed using an asymmetric window does not behave as expected — instead of increasing, it decreases. This inconsistency renders the method unreliable for anticipating ecological tipping points.

In conclusion, variance can be a useful tool for anticipating regime shifts, but its application is severely limited due to the smoothing window required for its computation. That said, in high-stakes ecosystems with strong human interest and frequent monitoring, the latency introduced by

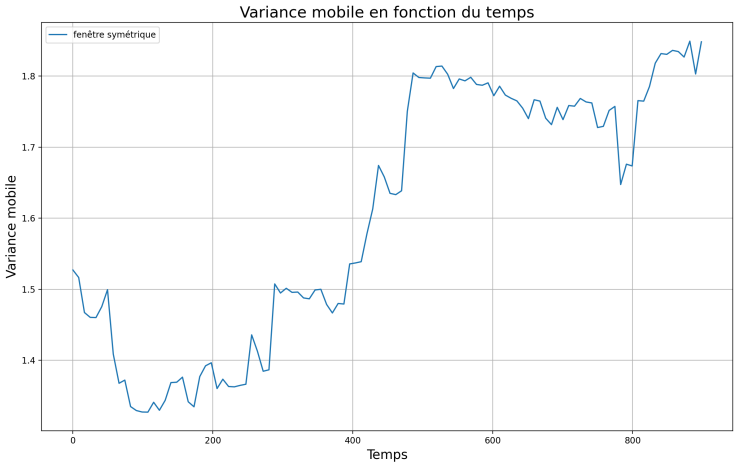

FIGURE 12 – Moving variance computed on one of the 1000 simulated stochastic series, prior to the tipping point, to evaluate the method under realistic conditions.

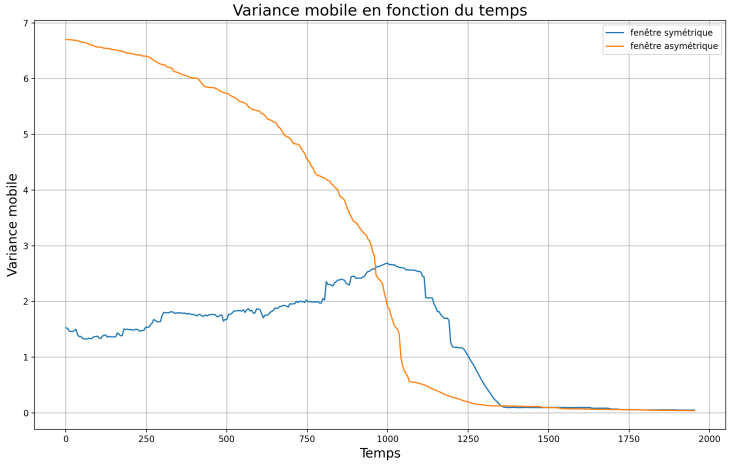

FIGURE 13 – Moving variance over a simulation before the tipping point, computed using both symmetric and asymmetric windows.

the windowing may be acceptable, making this technique still viable in those contexts.

4.2.2 Increasing autocorrelation in the time series

We start by visually assessing the increase in autocorrelation by plotting lag plots — specifically, plotting successive pairs (X_t, X_{t+1}) and examining their dispersion around the $y = x$ line. We split a time series of 500 values into sections of 100 values and observe how the points align in each segment.

We define three scenarios : Case 1 represents a stable system (Figure 14), Case 2 corresponds to a system near or undergoing a tipping point (Figure 15), and Case 3 occurs after the

tipping point (Figure 16).

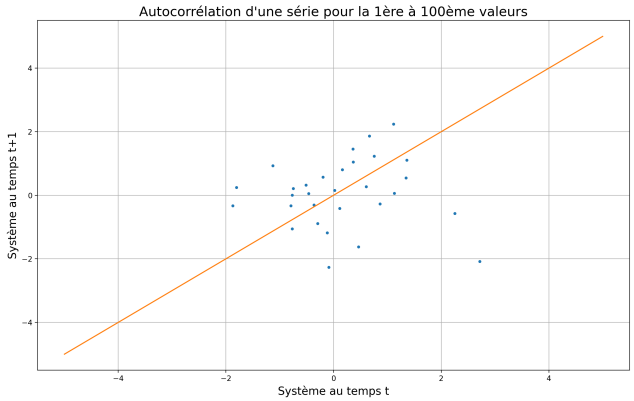

FIGURE 14 – Autocorrelation plot for values 1 to 100 in a simulation — system is stable, far from the tipping point.

In Figure 14, we observe low dispersion of points around the $y = x$ line, indicating a stable system, far from a tipping point.

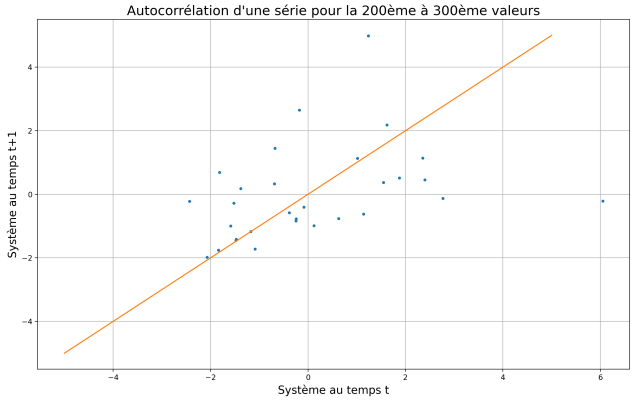

FIGURE 15 – Autocorrelation plot for values 200 to 300 — system approaching or undergoing a regime shift.

In Figure 15, the points are much more dispersed than in the previous case, suggesting that the system is nearing or has just undergone a tipping point.
Finally, in Figure 16, the points cluster very tightly around the $y = x$ line, which is consistent with a system that has transitioned to the low-density equilibrium state. We clearly observe a distinct difference across Figures 14, 15, and 16, corresponding to the three different phases.

However, all these observations are qualitative. To quantify the autocorrelation, we compute a moving lag-1 autocorrelation using a sliding window across the entire simulation. The results are shown in Figure 17.
In Figure 17, we observe a clear peak in autocorrelation at the tipping point. However, this simulation includes the tipping event itself, so the increase is expected. To further assess the predictive power of this method, we apply it to a simulation where the tipping point has not yet occurred

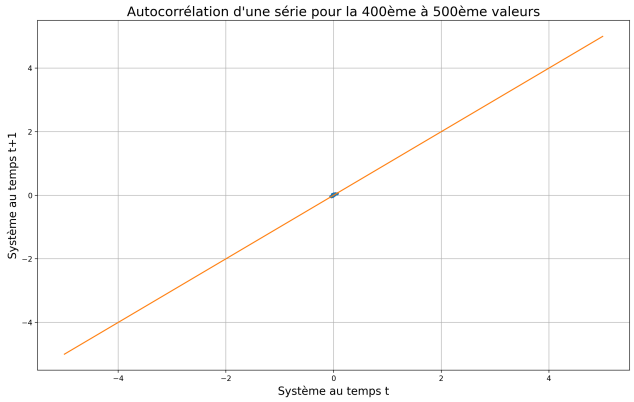

FIGURE 16 – Autocorrelation plot for values 400 to 500 — system has already passed the tipping point.

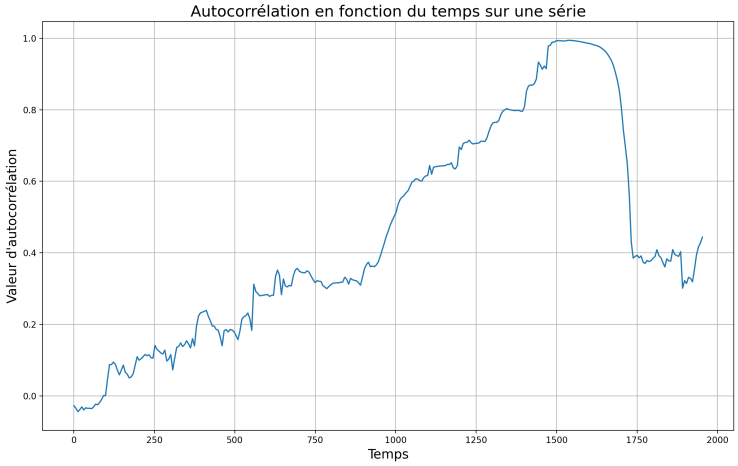

FIGURE 17 – Lag-1 autocorrelation over an entire simulation.

(Figure 18).

As seen in Figure 18, the autocorrelation value increases as the system approaches the tipping point. This suggests that lag-1 autocorrelation could be a reliable early warning signal in ecological models.

To confirm this, we repeat the analysis over the 1000 simulations conducted earlier and compute the mean autocorrelation over all these trajectories before the tipping point (Figure 19).

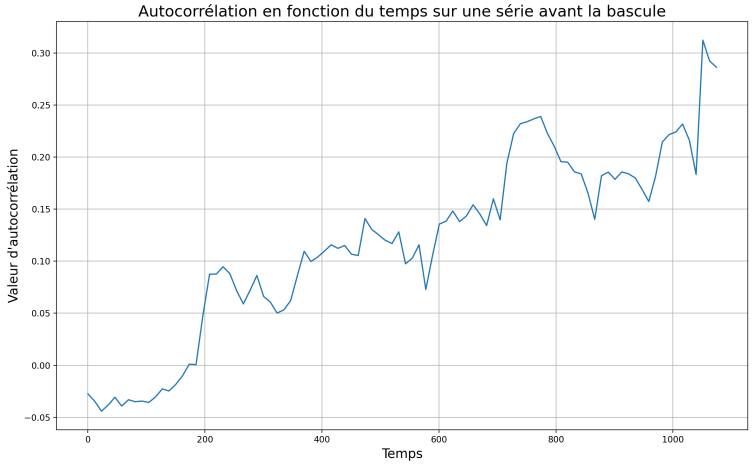

FIGURE 18 – Autocorrelation value in a simulation prior to the tipping point

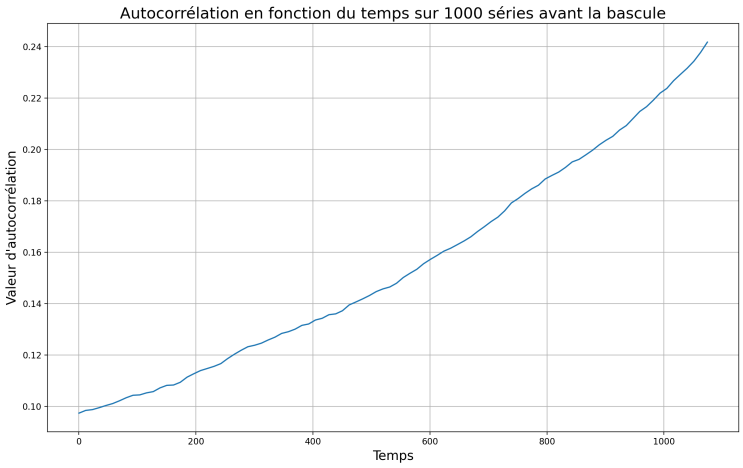

FIGURE 19 – Mean autocorrelation across 1000 simulations prior to the tipping point

Figure 19 shows that the autocorrelation is smoother and increases on average across 1000 simulations. We can therefore consider the increase in autocorrelation as a reliable indicator of an impending tipping point in an ecosystem. However, it is still necessary to define a threshold value beyond which a tipping point is considered imminent, prompting conservation action. Moreover, the same limitation applies as with the variance : the smoothing window used to compute autocorrelation prevents real-time knowledge of the system's current state.

5 Conclusion

Based on the results obtained, we observe that the stochastic model generally follows the trend of the deterministic model. However, due to its stochastic component, it enters the basin of attraction of the low-density equilibrium earlier, causing the system to shift sooner than in the deterministic case — i.e., for higher values of the driver parameter.

Regarding early warning signals, both the detection of increasing variance and increasing autocorrelation theoretically perform well. However, the calculation of both metrics requires access to future data points due to the symmetric smoothing windows. This introduces a delay between the computed indicators and the actual state of the system. Since tipping points are often abrupt, rapid, and irreversible, the use of these metrics for forecasting is limited. For future research, it would be useful to develop new methods to compute variance and autocorrelation without requiring future data.

6 References

Références

[1] Dakos, V. (2022). *Anticipating ecological surprises* [HDR thesis, University of Montpellier].

[2] Higham, J. (2001). An algorithmic introduction to numerical simulation of stochastic differential equations, *SIAM Review*, Vol. 43(3), 525–546. http ://www.jstor.org/stable/3649798

[3] Navarro-Boucksaux, L. (2024). *Studying ecosystem tipping points and their early-warning signals : A modeling approach* [Master's thesis, Aix-Marseille University].

[4] Simonoff, J. S. (1996). *Smoothing methods in statistics*. Springer.

[5] Steneck, R. et al. (2002). Kelp Forest Ecosystems : Biodiversity, Stability, Resilience and Future. *Environmental Conservation*, Vol. 29, 436–459.

7 Appendices

Appendix 1 :

$\frac{dx}{dT} = RN\left(1 - \frac{N}{K}\right) - \frac{AN^2}{B^2+N^2}P$, made dimensionless using $x = \frac{N}{B}$

$$
\begin{aligned}
x &= \frac{N}{B} \\
\frac{dx}{dT} &= \frac{dN}{dT} \cdot \frac{1}{B} \\
\frac{dx}{dT} &= \left(RN\left(1 - \frac{N}{K}\right) - \frac{AN^2}{B^2+N^2}P\right) \cdot \frac{1}{B} \\
\frac{dx}{dT} &= \frac{RN}{B} - \frac{RN}{KB} - \frac{AN^2}{B(B^2+N^2)}P \\
\frac{dx}{dT} &= Rx\left(1 - \frac{x}{K}\right) - \frac{APNx}{B(B^2+N^2)} \\
\frac{dx}{dT} &= Rx\left(1 - \frac{x}{K}\right) - \frac{APNx}{B(B^2+x^2B^2)} \\
\frac{dx}{dT} &= Rx\left(1 - \frac{x}{K}\right) - \frac{APNx}{B^2(1+x^2)}
\end{aligned}
$$

Now, assume $T = \frac{AP}{B}t$, hence $dT = \frac{AP}{B}dt$. Thus :

$$\frac{dx}{dt} = \frac{RB}{AP}x\left(1 - \frac{x}{K}\right) - \frac{x^2}{1+x^2}$$

Letting $r = \frac{RB}{AP}$ gives :

$$\frac{dx}{dt} = rx\left(1 - \frac{x}{K}\right) - \frac{x^2}{1+x^2}$$

Appendix 2 :

$$\begin{cases} r\left(1-\frac{x}{K}\right)=\frac{x}{1+x^2} \\ \frac{-r}{K}=\frac{1-x^2}{(1+x^2)^2} \end{cases}$$

$$\begin{cases} r\left(1-\frac{x}{K}\right)=\frac{x}{1+x^2} \\ r=-K\cdot\frac{1-x^2}{(1+x^2)^2} \end{cases}$$

$$\begin{cases} -K\cdot\frac{1-x^2}{(1+x^2)^2}\left(1-\frac{x}{K}\right)=\frac{x}{1+x^2} \quad (1) \\ r=-K\cdot\frac{1-x^2}{(1+x^2)^2} \quad (2) \end{cases}$$

Isolating K from Equation (1) :

$$\begin{aligned} \frac{x}{1+x^2} &= \frac{1-x^2}{(1+x^2)^2}(-K+x) \\ -K+x &= x\cdot\frac{(1+x^2)}{1-x^2} \\ K &= \frac{x(1-x^2)-x(1+x^2)}{1-x^2} \\ K &= \frac{2x^3}{x^2-1} \end{aligned}$$

Plugging this K into Equation (2) :

$$\begin{aligned} r &= -K\cdot\frac{1-x^2}{(1+x^2)^2} \\ r &= -\frac{2x^3}{x^2-1}\cdot\frac{1-x^2}{(1+x^2)^2} \\ r &= -2x^3\cdot\frac{-1+x^2}{(1-x^2)(1+x^2)^2} \end{aligned}$$

Appendix 3 :

Let us define a general model : $X_{t+1} = f(X_t) + \sigma\epsilon_t$, where ϵ_t follows a standard normal distribution. Ignoring the stochastic component, we assume :

$$X_{t+1} = f(X_t) + X_{eq}$$
$$X_{t+1} = f(X_{eq} + X_t) - X_{eq}$$

With a first-order Taylor expansion :

$$X_{t+1} = f(X_{eq}) + f'(X_{eq})X_t - X_{eq}$$

Since $f(X_{eq}) = X_{eq}$ in discrete time :

$$X_{t+1} = f'(X_{eq})X_t$$

Including the stochastic term and defining $a = f'(X_{eq})$:

$$X_{t+1} = aX_t + \sigma\epsilon_t$$

Assuming $P(X_0 = x_0) = 1$ with $x_0 = 0$ and independence between X_t and ϵ_t :

$$E(X_{t+1}) = aE(X_t) + \sigma E(\epsilon_t) = a^t E(X_0) = 0$$

Therefore :

$$
\begin{aligned}
Var(X_{t+1}) &= E(X_{t+1}^2) \\
&= E\left((aX_t + \sigma\epsilon_t)^2\right) \\
&= a^2E(X_t^2) + 2a\sigma E(X_t)E(\epsilon_t) + \sigma^2E(\epsilon_t^2) \\
&= a^2Var(X_t) + \sigma^2
\end{aligned}
$$

Assuming the stationary maximum variance $Var^*(X_t)$:

$$
\begin{aligned}
Var^*(X_t) &= a^2Var^*(X_t) + \sigma^2 \\
Var^*(X_t)(1 - a^2) &= \sigma^2 \\
Var^*(X_t) &= \frac{\sigma^2}{1 - a^2}
\end{aligned}
$$

Thus, as $a \to 1$, $Var^*(X_t) \to \infty$. Since $a = 1$ corresponds to the tipping point, we observe an increase in variance as the system approaches a regime shift.